

**Multiwalled Carbon Nanotubes Anode in Lithium-Ion Battery with LiCoO<sub>2</sub>,  
Li[Ni<sub>1/3</sub>Co<sub>1/3</sub>Mn<sub>1/3</sub>]O<sub>2</sub> and LiFe<sub>1/4</sub>Mn<sub>1/2</sub>Co<sub>1/4</sub>PO<sub>4</sub> Cathodes**

Daniele Di Lecce<sup>a</sup>, Paolo Andreotti<sup>a</sup>, Mattia Boni<sup>a</sup>, Giulia Gasparro<sup>a</sup>, Giulia Rizzati<sup>a</sup>, Jang-Yeon Hwang<sup>b</sup>, Yang-Kook Sun<sup>b,\*</sup> and Jusef Hassoun<sup>a,\*</sup>

<sup>a</sup> University of Ferrara, Department of Chemical and Pharmaceutical Sciences, Via Fossato di Mortara, 17, 44121, Ferrara, Italy

<sup>b</sup> Department of Energy Engineering, Hanyang University, Seoul 133-791, South Korea

\* Corresponding authors: [jusef.hassoun@unife.it](mailto:jusef.hassoun@unife.it), [yksun@hanyang.ac.kr](mailto:yksun@hanyang.ac.kr)

**Abstract**

Multiwalled carbon nanotubes (MWCNTs) are studied for the first time as the anode in lithium-ion batteries using LiCoO<sub>2</sub>, Li[Ni<sub>1/3</sub>Co<sub>1/3</sub>Mn<sub>1/3</sub>]O<sub>2</sub> and LiFe<sub>1/4</sub>Mn<sub>1/2</sub>Co<sub>1/4</sub>PO<sub>4</sub> cathodes. The anode material has a partially graphitic structure and nanotube morphology, which ensure stable cycling, Coulombic efficiency exceeding 99% as well as remarkable rate-capability in lithium half-cell, and suggest the compatibility for full-cell application. The performance of each lithium-ion array appears strongly related to the different structural, morphological and electrochemical features of the positive electrodes. The study in full-cell of the MWCNT anode, to date mostly investigated in lithium half-cell, is therefore performed under various conditions. The MWCNT/Li[Ni<sub>1/3</sub>Co<sub>1/3</sub>Mn<sub>1/3</sub>]O<sub>2</sub> combination reveals promising behavior in terms of cycling stability, reversible capacity and Coulombic efficiency, which well demonstrates the potential suitability of MWCNTs as anodes in lithium-ion cell.

**Keywords**

Multiwalled carbon nanotubes, LiCoO<sub>2</sub>, Li[Ni<sub>1/3</sub>Co<sub>1/3</sub>Mn<sub>1/3</sub>]O<sub>2</sub>, LiFe<sub>1/4</sub>Mn<sub>1/2</sub>Co<sub>1/4</sub>PO<sub>4</sub>, Li-ion battery

## Introduction

Current research on lithium-ion batteries is focusing on novel electrode materials with enhanced electrochemical features with respect to the conventional ones. Various studies aimed at improving the cell performance to match the needs of a wide array of emerging technologies, ranging from new-generation portable electronics to electric vehicles and small-/medium-scale grid energy storage.<sup>1</sup> Accordingly, new cathode materials characterized by high specific capacity and/or working voltage, such as advanced transition metal oxides<sup>2-4</sup> and polyanionic compounds,<sup>5-7</sup> have been recently investigated with promising results. The studies revealed the key role of the material optimization in terms of composition, structure and morphology to enhance the cathode performance. As for the anode side, alternative, high-capacity electrode materials reacting with lithium by insertion, conversion or alloying have been widely studied.<sup>8</sup> Several carbonaceous materials with different morphologies, *i.e.*, zero- (0D), one- (1D), two- (2D), and three-dimensional structures, have been reported as electrodes for battery application. Their performances in lithium-ion cell are strongly related to the structural and morphological features.<sup>9</sup> Composites materials based on semi-metallic and metallic elements or metal oxides have been recently proposed as high-performance anodes reacting by alloying or conversion, respectively.<sup>10-</sup><sup>16</sup> Alloy-based electrodes typically have low working voltage *vs* Li<sup>+</sup>/Li and high theoretical capacity, especially those based on IV group elements, but suffer from huge volume change upon Li-(de)alloying, which may leads to material pulverization throughout cycling. Therefore, alloying nanoparticles are generally entrapped within either active or inactive matrixes able to buffer the volume variation, such as carbon, which may decrease the practical capacity. As for metal oxide-based anodes, the multiple-electron conversion reaction ensures higher reversible capacity than the insertion one. However, such materials exhibit large voltage hysteresis and volume variation,

as well as high working potential *vs*  $\text{Li}^+/\text{Li}$ , which may affect the energy density of the lithium-ion cell.<sup>8</sup> Moreover, both alloying and conversion-type anodes are typically characterized by large first-cycle irreversible capacity, which requires electrode pre-treatments before full-cell assembly.<sup>17</sup>

Among the carbonaceous materials, carbon nanotubes (CNTs) have been characterized as possible anodes for lithium-ion battery in several literature works.<sup>18–23</sup> Indeed, since the first report on CNTs in 1991,<sup>24</sup> the reversible electrochemical insertion of  $\text{Li}^+$  into single-walled and multi-walled CNTs (SWCNTs and MWCNTs, respectively) has been thoroughly demonstrated. Lithium ions can diffuse into stable sites either on the outer or the inner surface of a single CNT graphene layer, thereby leading to a larger  $\text{Li}^+$  uptake than  $\text{LiC}_6$ . Furthermore, lithium ions can be inserted into interstitial sites of close-packed SWCNT bundles and within the graphene layers of MWCNTs.<sup>25</sup> Therefore, the achievable lithium-ion capacity of CNT materials is strongly related to their morphology.<sup>26</sup> In particular, highly-defective, short CNTs exhibit remarkable capacity. However, structure defects also increase the irreversible capacity, and lead to large voltage hysteresis as well as to high working voltage *vs*  $\text{Li}^+/\text{Li}$ ,<sup>21,27,28</sup> which are serious drawbacks for lithium-ion battery application. On the other hand, graphitic MWCNTs usually ensure better cycling performances with high Coulombic efficiency through electrochemical processes at low voltage *vs*  $\text{Li}^+/\text{Li}$ , however with relatively low reversible capacity.<sup>28</sup> Despite the remarkable performances in terms of specific capacity reported so far,<sup>29–32</sup> several unsolved issues still limit the application of CNTs as electrodes. Accordingly, only a few papers reported the electrochemical characterization in full-cell of CNT anodes,<sup>33</sup> while the scientific community has mostly focused the attention on the electrochemical study in lithium half-cell.<sup>28</sup> Therefore, further work is needed to demonstrate the applicability of such materials as negative electrodes.

Following this trend, we investigated the use of a MWCNT anode in lithium-ion cells with three cathode materials differing by structure, morphology and electrochemical behavior, *i.e.*, the  $\text{LiCoO}_2$ <sup>34</sup> and  $\text{Li}[\text{Ni}_{1/3}\text{Co}_{1/3}\text{Mn}_{1/3}]\text{O}_2$ <sup>35</sup> layered oxides and the  $\text{LiFe}_{1/4}\text{Mn}_{1/2}\text{Co}_{1/4}\text{PO}_4$ <sup>36</sup> olivine. All the materials have been comparatively characterized in terms of structure, morphology, composition and electrochemical properties. The features of each lithium-ion array allowed the study of the electrochemical behavior of the MWCNT anode in several experimental conditions. The results of this work are therefore expected to provide further knowledge on the use of CNTs as negative electrode in lithium-ion battery.

## Experimental Section

Multiwalled carbon nanotubes (MWCNTs) purchased from Sigma Aldrich (99.8% purity) were annealed for 12 h at 750 under a nitrogen flow in order to remove possible impurities, adsorbed water and undesired surface functional groups (sample MWCNT').  $\text{LiCoO}_2$  (LCO) was synthesized by the solid-state method according to an already reported recipe.<sup>34</sup>  $\text{Li}[\text{Ni}_{1/3}\text{Co}_{1/3}\text{Mn}_{1/3}]\text{O}_2$  (NCM) was synthesized by co-precipitation of  $(\text{Ni}_{1/3}\text{Co}_{1/3}\text{Mn}_{1/3})(\text{OH})_2$  in a continuous stirred tank reactor (CSTR) followed by calcination of the precursor with LiOH, according to an already reported procedure.<sup>35</sup>  $\text{LiFe}_{1/4}\text{Mn}_{1/2}\text{Co}_{1/4}\text{PO}_4$  was prepared by low-temperature solvothermal method and C-coated by pyrolysis of sucrose as previously reported.<sup>36</sup>

X-ray diffraction patterns were recorded through a Bruker D8 Advance diffractometer equipped with a  $\text{CuK}\alpha$  source. Sample morphology and composition were analyzed by scanning electron microscopy (SEM), SEM-energy dispersive X-ray spectroscopy (EDS) and transmission electron microscopy (TEM). SEM and SEM-EDS were performed through a Zeiss EVO 40 microscope with a  $\text{LaB}_6$  thermoionic gun, equipped with a X-ACT Cambridge Instrument analyzer for EDS. TEM imaging was carried out by using a Zeiss EM 910 instrument equipped with a

tungsten thermoionic electron gun. The sample for TEM analysis was suspended in water, sonicated and deposited onto a Formvar support film applied on a Cu grid. Selected area diffraction pattern (SADP) was recorded through the former microscope.

Electrode films of MWCNT', LCO, NCM, and LFMCP supported on current collector foils were made by casting through doctor blade. Slurries of active material, poly(vinylidene fluoride) binder (PVDF 6020, Solef Solvay), and Super P (Timcal) conductive agent in N-methyl pyrrolidone (NMP, Sigma-Aldrich) in the weight ratio of 8:1:1 were prepared and deposited on the current collector foils. The coated foils were dried 3 hours at about 70 °C under air in order to evaporate the NMP solvent and then cut into electrode disks with diameter of either 10 mm or 14 mm for either T-cell or coin-cell use, respectively. The electrode disks were dried overnight under vacuum at 110 °C before use. Cu foils (thickness of 25 μm, MTI Corporation) were used as the current collectors for MWCNT'; Al foils (thickness of 15 μm, MTI Corporation) were used as the current collectors for LCO and NCM; carbon foam sheets (thickness of 454 μm, MTI Corporation) were used as the current collectors for LFMCP. The carbon sheet support may enhance the performance of olivine cathode materials as previously reported.<sup>37,38</sup> The active material loadings of the electrodes cycled in lithium half-cell were about 5 mg cm<sup>-2</sup> for LCO and NCM, 6 mg cm<sup>-2</sup> for LFMCP, and 1 mg cm<sup>-2</sup> for MWCNT'. The active material loadings of LCO, NCM and LFMCP were lowered to about 2.3, 3.1 and 1.5 mg cm<sup>-2</sup>, respectively, in order to match the anode capacity in full-cell based on our previous reports.

The electrochemical tests were performed by using an electrolyte solution of 1M LiPF<sub>6</sub> in ethylene carbonate/dimethyl carbonate (EC/DMC 1/1 by weight; LP30, battery grade, BASF), which was imbibed by a Whatman glass-fiber separator. Coin-cells 2032 and T-type, polyethylene cells were assembled in an Ar-filled glovebox (O<sub>2</sub> and H<sub>2</sub>O content lower than 1 ppm) by stacking

anode, separator soaked with the electrolyte, and cathode. Coin-cells were used for the cycling tests in half-cell (two-electrode cell). T-cells were used for the cyclic voltammetry tests of the electrodes (three-electrode cell) and the galvanostatic cycling of the full-cells (two-electrode cell). Fig. S1 in the Supporting Information shows a schematic diagram of the T-cell.

The cyclic voltammetry experiments were performed on three-electrode cells using lithium-metal counter and reference electrodes through a VersaSTAT MC Princeton Applied Research (PAR). The cyclic voltammetry measurements were carried out at a scan rate of  $0.1 \text{ mV s}^{-1}$ . The following potential ranges were used of the tests:  $0.01 - 2 \text{ V vs Li}^+/\text{Li}$  for MWCNT';  $2.7 - 4.4 \text{ V vs Li}^+/\text{Li}$  for both LCO and NCM;  $2 - 4.9 \text{ V vs Li}^+/\text{Li}$  for LFMCP.

Galvanostatic cycling experiments were performed on two-electrode cells through a MACCOR series 4000 battery tester. MWCNT' was cycled in lithium half-cell within the  $0.01 - 2 \text{ V}$  voltage range at a current rate of  $C/3$  ( $124 \text{ mA g}^{-1}$ ; 1C was referred to the theoretical capacity of graphite, *i.e.*,  $372 \text{ mAh g}^{-1}$ ). LCO was cycled in lithium half-cell within the  $2.7 - 4.1 \text{ V}$  voltage range at a current rate of  $C/2$  ( $137 \text{ mA g}^{-1}$ ; 1C was referred to the theoretical capacity for the exchange of 1 mol of  $\text{Li}^+$  for 1 mol of  $\text{LiCoO}_2$ , *i.e.*,  $274 \text{ mAh g}^{-1}$ ). NCM was cycled in lithium half-cell within the  $2.7 - 4.4 \text{ V}$  voltage range at a current rate of  $C/2$  ( $140 \text{ mA g}^{-1}$ ; 1C was referred to the theoretical capacity for the exchange of 1 mol of  $\text{Li}^+$  for 1 mol of  $\text{Li}[\text{Ni}_{1/3}\text{Co}_{1/3}\text{Mn}_{1/3}]\text{O}_2$ , *i.e.*,  $280 \text{ mAh g}^{-1}$ ). LFMCP was cycled in lithium half-cell within the  $2 - 4.9 \text{ V}$  voltage range at a current rate of  $C/5$  ( $34 \text{ mA g}^{-1}$ ; 1C was referred to the theoretical capacity for the exchange of 1 mol of  $\text{Li}^+$  for 1 mol of  $\text{LiFe}_{1/4}\text{Mn}_{1/2}\text{Co}_{1/4}\text{PO}_4$ , *i.e.*,  $170 \text{ mAh g}^{-1}$ ). Rate capability tests were performed by galvanostatic cycling in lithium half-cell at current rates of  $C/10$ ,  $C/8$ ,  $C/5$ ,  $C/3$ ,  $C/2$ , 1C, 2C, 5C; the same voltage ranges used for the single-current tests were employed.

Lithium-ion full-cells were assembled by using an electrochemically-activated MWCNT' electrode and LCO, NCM and LFMCP cathodes. The negative-to-positive ratios (N/P) of the full-cells in terms of capacity were 1.9, 1.3 and 1.5 for LCO, NCM and LFMCP, respectively. We have set the N/P ratio taking into account the full expected capacity of each electrode, *i.e.*, 140 mAh g<sup>-1</sup> for LCO, 160 mAh g<sup>-1</sup> for NCM, 170 mAh g<sup>-1</sup> for LFMCP, and 380 mAh g<sup>-1</sup> for MWCNT'. The electrochemical activation of the anode was performed by galvanostatic cycling in lithium half-cell at a C/5 rate (1C = 372 mA g<sup>-1</sup>) for 5 cycles and following charge of the cell up to 0.9 V. LFMCP cathode was pre-cycled for 5 cycles at C/5 (1C=170 mA g<sup>-1</sup>) before use, while LCO, NCM were used without pre-cycling. Afterwards, the cell was disassembled in order to recover the MWCNT' electrode, which was used in full-cell without any further treatment. The MWCNT'/LCO cell was cycled within the 2.5 – 4 V range at a C/2 rate (137 mA g<sup>-1</sup> with respect to the cathode); the MWCNT'/NCM cell was cycled within the 2.5 – 4.3 V range at a C/2 rate (140 mA g<sup>-1</sup> with respect to the cathode); the MWCNT'/LFMCP cell was cycled within the 2 – 4.7 V range at a C/2 rate (85 mA g<sup>-1</sup>).

All the electrochemical tests were performed at 23 °C.

## **Results and discussion**

As above mentioned, structure and morphology of the of MWCNTs electrode material play a remarkable role in determining its lithium exchange ability. Literature data indicated wide working voltage and specific capacity ranges for different CNT samples, depending on the graphitic character, the number of defects, the nanotube length and thickness, as well as the metallic/semiconducting character of the material. Thus, highly graphitic, thick CNT sample generally exhibit smaller voltage hysteresis, limited first-cycle inefficiency, higher Coulombic efficiency, however a lower capacity upon cycling in lithium cell compared to thin and disordered

one<sup>25,28</sup>. Structure and morphology of the MWCNT' material have been herein investigated by coupling XRD and electron microscopy (Fig. 1). The comparison of the XRD pattern of the sample with the reference data sheet of graphite carbon (PDF # 751621, see Fig. 1a) reveals its partially graphitic structure. The SEM and TEM images of Fig. 1b-e clearly show a sample formed by micrometric rods with a diameter ranging from 100 to 200 nm, while the SADP of the TEM (inset of Fig. 1e) further indicates the crystalline structure of the material, thus in agreement with the XRD results. These structural and morphological features can actually ensure crucial requirements for full-cell application such as high Coulombic efficiency, low capacity fading and low operating voltage owing to the graphitic character,<sup>28,39</sup> as indeed confirmed by the electrochemical results reported in Fig. 2. Fig. S2 in the Supporting Information shows the FT-IR spectra of the MWCNTs before and after annealing (samples MWCNT pristine and MWCNT'). The graph related to the pristine material reveals broad peaks at 3415 and 1620  $\text{cm}^{-1}$ , which can be attributed respectively to O-H and C=O stretching vibrations of possible carboxyl functional groups or absorbed water, as well as a peak at 1080  $\text{cm}^{-1}$  assigned to the C-O stretching vibration. The presence of these peaks has been already observed in literature and related to the possible oxidation of the MWCNTs with introduction of COOH groups on the surface of MWCNTs.<sup>40</sup> Further functionalities may be indicated by the peak around 2500  $\text{cm}^{-1}$ , likely ascribed to the C-H stretching mode,<sup>41</sup> and the peak at about 1300  $\text{cm}^{-1}$  probably due to C-O-C stretching mode.<sup>42</sup> Minor differences are revealed by the spectrum of MWCNT', in particular for the peak at 1080  $\text{cm}^{-1}$  (C-O stretching) and 2500  $\text{cm}^{-1}$  (C-H stretching) which become smaller.

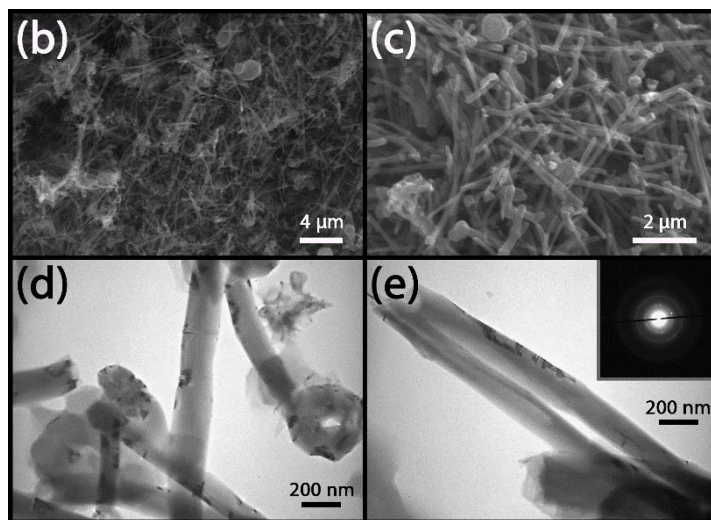
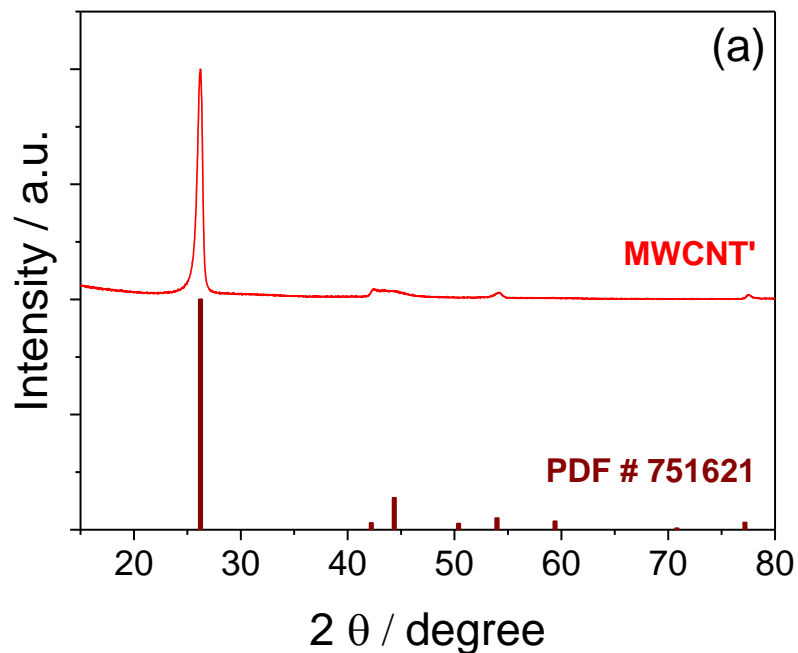


**Figure 1.** (a) XRD patterns of the MWCNT' sample and carbon reference (PDF # 751621). (b-e) Electron microscopy analyses of the MWCNT' sample by (d, c) SEM at different magnifications and (d, e) TEM; SADP in panel e inset.

Fig. 2a shows the cyclic voltammetry of the MWCNT' electrode in three-electrode lithium cell. The first cycle reveals a small peak at about 0.7 V vs  $\text{Li}^+/\text{Li}$  upon reduction indicating an irreversible process, which is attributed to the solid electrolyte interphase (SEI) formation.<sup>43,44</sup>

Moreover, Fig. 2a shows reversible electrochemical reactions mostly occurring below 0.3 V vs Li<sup>+</sup>/Li, ascribed to the Li<sup>+</sup> (de)insertion within the MWCNT' electrode. The full overlapping of the curves by the subsequent cycles further suggests a highly reversible electrochemical processes at the MWCNTs. The electrode has been studied by galvanostatic cycling in lithium half-cell at several current rates (Fig. 2b) as well as at a single current rate upon 100 cycles (Fig. 2c, d). The rate capability test shows only minor decrease on the reversible capacity of the MWCNT' electrode by current increase from C/10 to C/2 rates (1C = 372 mA g<sup>-1</sup>); indeed, the cell delivers a reversible capacity of 372, 364, 355, and 345 mAh g<sup>-1</sup> at C/10, C/5, C/3, and C/2 rates, respectively. Further current rise leads to a capacity decrease to 301, 192, and 99 mAh g<sup>-1</sup>, respectively delivered at 1C, 2C, and 5C rates. The cell recovers the initial capacity of 372 mAh g<sup>-1</sup> as the current is decreased to C/10 rate at the 22<sup>nd</sup> cycle. Fig. S3 in the Supporting Information indicates slight overvoltage during the rate capability test, due to the current increase. Panels c and d of Fig. 2 show the results of a cycling test at a C/3 rate (1C = 372 mA g<sup>-1</sup>) over 100 cycles in terms of voltage curves and cycling behavior, respectively. The cell exhibits a sloping voltage profile at about 0.7 V upon the first discharge (see Fig. 2c inset), ascribed to the above mentioned SEI formation,<sup>43,44</sup> which leads to an irreversible capacity of 201 mAh g<sup>-1</sup>. This plateau does not occur by the subsequent cycles (Fig. 2c), and a large fraction of the Li<sup>+</sup> insertion/deinsertion occurs below 0.5 V, thus in agreement with the cyclic voltammetry. This reversible trend may be partially related to the high crystallinity of the MWCNT' material suggested by XRD and SADP.<sup>39</sup> On the other hand, a small fraction of the reversible electrochemical process takes place through a sloppy voltage profile above 0.5 V both upon discharge and charge. This feature may be actually attributed to Li<sup>+</sup> uptake in defective and/or non-graphitic carbon sites.<sup>25,45</sup> As already suggested by the overlapping of the voltage profiles in cyclic voltammetry, Fig. 2d indicates a remarkably stable reversible capacity

approaching  $380 \text{ mAh g}^{-1}$  over 100 cycles at C/3 ( $1C = 372 \text{ mA g}^{-1}$ ) with an average Coulombic efficiency of 99.6% after few stabilization cycles.

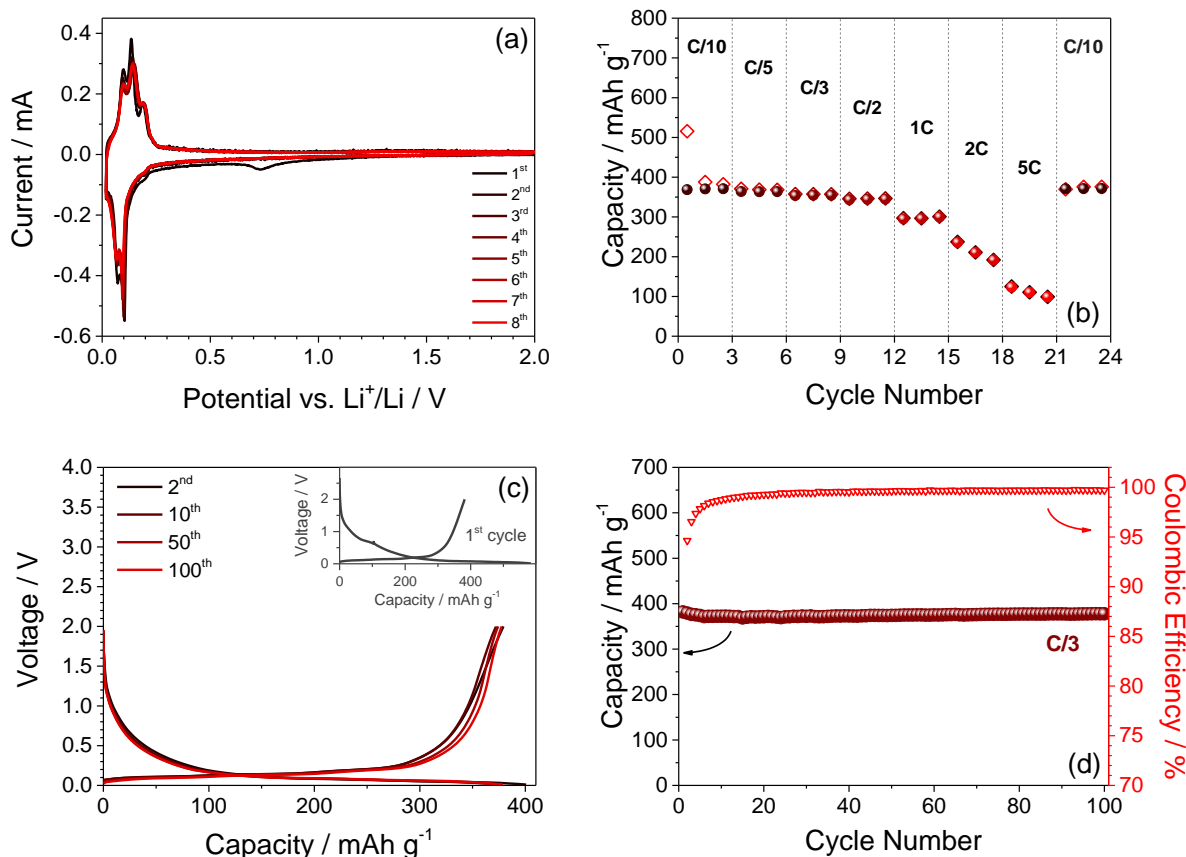


**Figure 2.** Electrochemical characterization of the MWCNT' sample. **(a)** Cyclic voltammetry in three-electrode T-cell using lithium counter and reference electrodes at a scan rate of  $0.1 \text{ mV s}^{-1}$ . **(b)** Rate capability test in lithium half-cell at C/10, C/5, C/3, C/2, 1C, 2C, and 5C rates ( $1C = 372 \text{ mAh g}^{-1}$ ). **(c, d)** Galvanostatic cycling test in lithium half-cell at a C/3 rate in terms of **(c)** voltage profiles and **(d)** cycling trend (specific capacity and Coulombic efficiency on the left and right y-axes, respectively); 1<sup>st</sup> voltage profile in panel **c** inset.

The annealing actually improves the electrode performance in lithium cell, as shown in Fig. S4 in the Supplementary Information. Indeed, Fig. S4 clearly reveals a capacity increase after the thermal treatment, as well as an increase of the electrochemical processes associated with

defective and/or non-graphitic carbon. The MWCNT' material exhibits promising electrochemical behavior aimed at application in lithium-ion full-cells with insertion cathodes, that is, (i) relatively low electrochemical potential for lithium exchange, (ii) low voltage hysteresis, and (iii) stable cycling with high Coulombic efficiency.<sup>1,8</sup> Nevertheless, large part of the literature has focused on the characterization and electrochemical evaluation of single- and multiwalled CNTs only in lithium half-cell, even with remarkably high specific capacity values,<sup>28-32</sup> rather than in full-cell. Therefore, we have studied the MWCNT' electrode as the anode in lithium-ion cells with three cathode materials differing by structure, morphology and, accordingly, electrochemical features, namely LCO, NCM layered oxides and LFMCP olivine (see the Experimental section for sample acronym). The XRD patterns of the samples reported in Fig. 3a show the expected reflections of the layered structure of LCO and NCM (PDF # 750532) as well as those of the olivine structure of LFMCP (PDF # 832092). The LCO sample appears formed by irregular aggregates of micrometric particles, as shown by SEM in panels b and c of Fig. 3. Instead, NCM is homogeneously composed of round-shaped aggregates with average diameter of about 10  $\mu\text{m}$  and sub-micrometric primary particles (panels e and f of Fig. 3). On the other hand, olivine cathode materials typically have a sub-micrometric morphology able to mitigate the low electronic conductivity and slow lithium-ion transport by shortening the electron and lithium diffusion pathways.<sup>46,47</sup> Accordingly, the LFMCP has been synthesized into regular sub-micrometric particles, as shown in panels h and i of Fig. 3, and coated by a thin carbon layer in order to improve the electrochemical performances<sup>36</sup> (see the Experimental section for further details). The atomic composition of the samples and the homogeneous elemental distribution have been confirmed by SEM-EDS (see panels d, g and l of Fig. 3 and the related insets, reporting the elemental analyses for LCO, NCM and LFMCP, respectively).

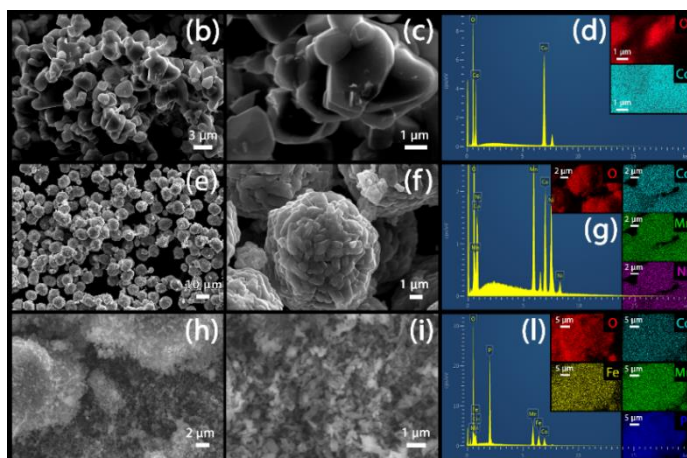
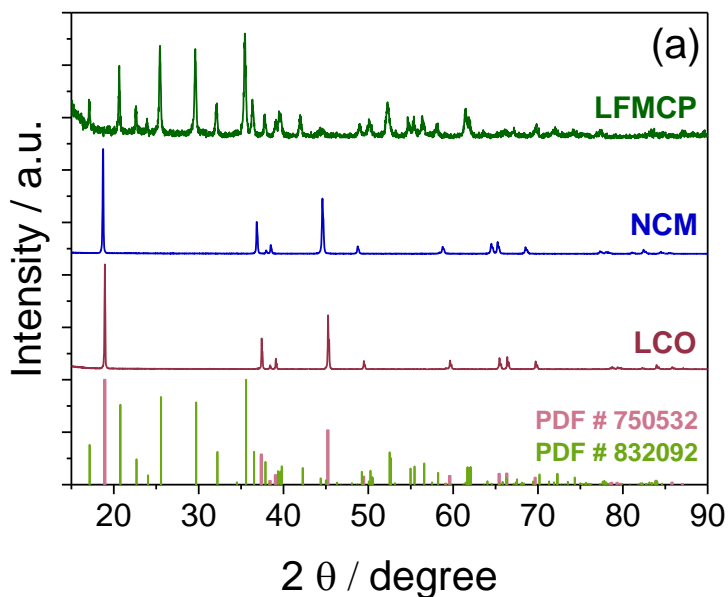


**Figure 3.** (a) XRD patterns of LCO, NCM and LFMCP as well as reference data of LiCoO<sub>2</sub> (PDF # 750532) and LiFePO<sub>4</sub> (PDF # 832092). (b-l) Electron microscopy analyses of (b-d) LCO, (e-g) NCM and (h-l) LFMCP. In detail: (b-c, e-f, h-i) SEM images at different magnification of the samples; (d) SEM-EDS of LCO and elemental mapping of O and Co in inset; (g) SEM-EDS of NCM and elemental mapping of O, Co, Mn, and Ni in inset; (l) SEM-EDS of LFMCP and elemental mapping of O, Co, Fe, Mn, and P in inset.

Fig. 4 compares the electrochemical features of LCO, NCM and LFMCP in terms of cyclic voltammetry (panel a), rate capability (panel b), and cycling behavior (panels c and d). Fig. 4a

shows the cyclic voltammetry of the electrode materials in three-electrode lithium cell. The top panel, related to LCO, reveals the typical response of  $\text{LiCoO}_2$  materials, characterized by three peaks upon both oxidation and reduction scans,<sup>48</sup> which occur at 3.96, 4.07 and 4.19 V *vs*  $\text{Li}^+/\text{Li}$  during lithium extraction and at 3.87, 4.04 and 4.16 V *vs*  $\text{Li}^+/\text{Li}$  during lithium insertion. In particular, the peaks above 4.1 V *vs*  $\text{Li}^+/\text{Li}$  have been attributed to the transition from a hexagonal to a monoclinic phase, which leads to structural degradation in  $\text{LiCoO}_2$  electrodes,<sup>34,49–51</sup> Accordingly, the charge cutoff has been set at 4.1 V for the galvanostatic cycling tests in lithium half-cell (Fig. 4b-d). On the other hand, NCM exhibits reversible lithium intercalation up to 4.4 V *vs*  $\text{Li}^+/\text{Li}$  through voltammetry peaks centered at 3.78 V *vs*  $\text{Li}^+/\text{Li}$  upon charge and 3.72 V *vs*  $\text{Li}^+/\text{Li}$  upon discharge. LFMCP shows the electrochemical activity of the  $\text{Fe}^{3+}/\text{Fe}^{2+}$ ,  $\text{Mn}^{3+}/\text{Mn}^{2+}$  and  $\text{Co}^{3+}/\text{Co}^{2+}$  redox couples within the olivine lattice at 3.56, 4.26 and 4.74 V *vs*  $\text{Li}^+/\text{Li}$  during oxidation and 3.46, 3.96 and 4.61 V *vs*  $\text{Li}^+/\text{Li}$  during reduction. Therefore, the LFMCP electrode has been cycled in lithium half-cell within the wide 2 – 4.9 V range in order to exploit the electrochemical processes due to the three transition metals.

Fig. 4b shows the results of rate capability tests of the LCO, NCM and LFMCP electrodes in lithium half-cell. Herein, the 1C rate has been calculated by taking into account the extraction of 1 mol of  $\text{Li}^+$  per mol of active material (see the Experimental section for further details). The LCO material delivers a reversible capacity of 126, 124, 120, 113, and 93 mAh  $\text{g}^{-1}$  at C/10, C/8, C/5, C/3, and C/2 rates (1C = 274 mA  $\text{g}^{-1}$ ). It is noteworthy that the relatively low charge cutoff (4.1 V), which is close to the working voltage of LCO, leads to full electrode deactivation as the current increases to 1C owing to cell polarization (see the voltage profiles of the rate capability tests in Fig. S5 of the Supporting Information). NCM, in contrast, shows the best rate performance among the investigated cathodes, with capacity of 168, 164, 160, 155, 145, 130, 104, and 60 mAh

$\text{g}^{-1}$  at C/10, C/8, C/5, C/3, C/2, 1C, 2C, and 5C rates ( $1\text{C} = 280 \text{ mA g}^{-1}$ ). As for LFMCP, the rate capability test reveals lower capacity at slow rates than the layered materials: the reversible capacity decreases from  $120 \text{ mAh g}^{-1}$  at C/10 to 106, 94, 83, 68,  $\text{mAh g}^{-1}$  at C/8, C/5, C/3, and C/2 rates ( $1\text{C} = 170 \text{ mA g}^{-1}$ ). However, the LFMCP electrode exhibits better high-rate behavior than LCO, by delivering 53, 35, and  $23 \text{ mAh g}^{-1}$  at 1C, 2C, and 5C rates. All the cells recover the initial capacity as the current decreases to C/10 at the 25<sup>th</sup> cycle.

Taking into account the rate capability results, we have tested the layered materials at a current rate of C/2 and the LFMCP olivine at a current rate of C/5. Such current rates ensure stable reversible capacity of about 110, 155 and  $100 \text{ mAh g}^{-1}$  for LCO, NCM and LFMCP, respectively, as shown in panels c and d of Fig. 4. The comparison of voltage curves provided in Fig. 4c illustrates the different characteristics of the electrode materials in terms of working voltage and delivered capacity, which are expected to strongly affect the behavior of the corresponding full-cells with the MWCNT' anode. Indeed, as already mentioned, LCO exchanges up to about 0.5 moles of  $\text{Li}^+$  ions within a narrow voltage window centered at 4 V, while NCM can reversibly (de)intercalate a larger amount of lithium between 3.5 and 4.4 V.<sup>52</sup> Furthermore, LFMCP shows a broad voltage range for the (de)insertion of about 0.6 moles of  $\text{Li}^+$  per mol of  $\text{LiFe}_{1/4}\text{Mn}_{1/2}\text{Co}_{1/4}\text{PO}_4$ , with working voltage at the stability limit of conventional electrolytes.<sup>53</sup> Accordingly, the olivine cathode exhibits lower Coulombic efficiency upon cycling than the layered materials, as shown in Fig. 4b. This issue may particularly affect the electrode mass balance in full-cell.<sup>1</sup>

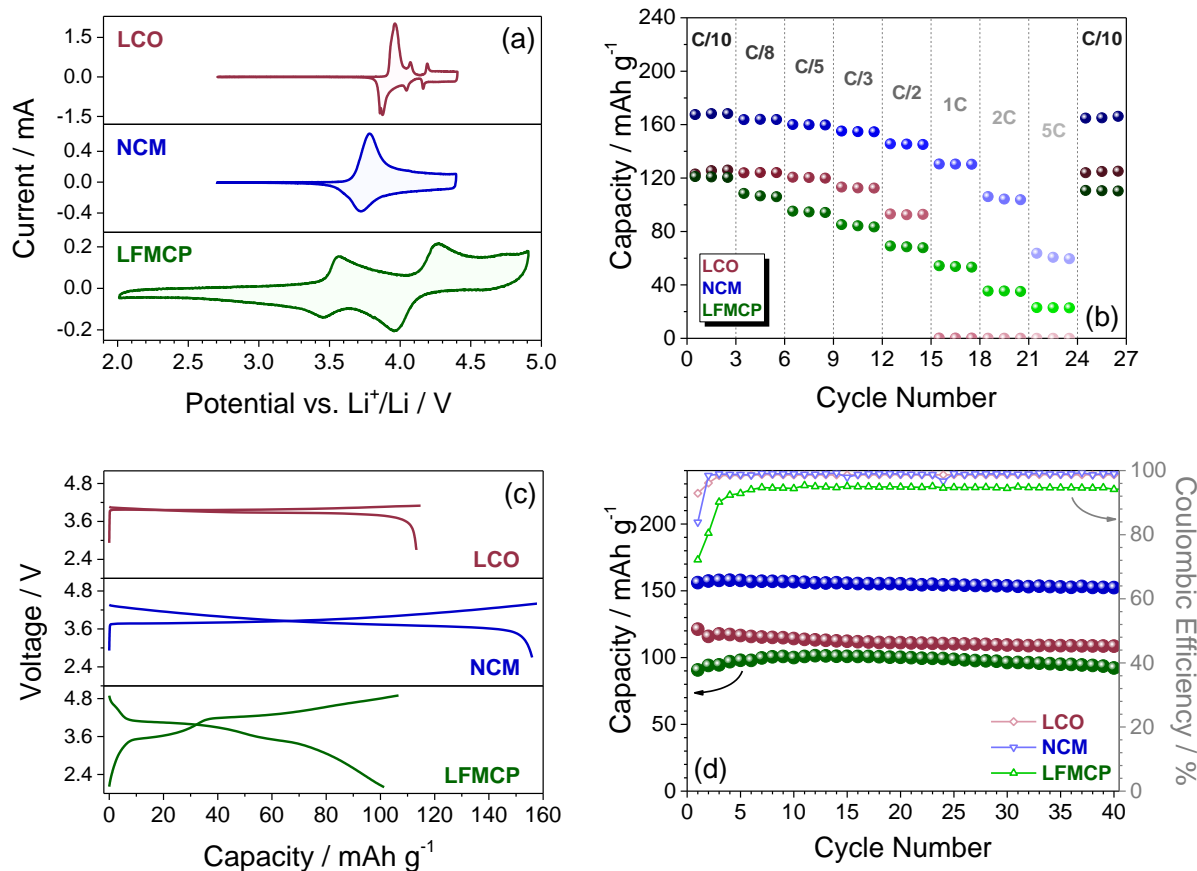


**Figure 4.** Electrochemical characterization of LCO, NCM and LFMCP. **(a)** Cyclic voltammetry in three-electrode T-cell using lithium counter and reference electrodes at a scan rate of 0.1 mV s<sup>-1</sup>. **(b)** Rate capability tests in lithium half-cell at C/10, C/8, C/5, C/3, C/2, 1C, 2C, and 5C rates (1C = 274; 280; 170 mAh g<sup>-1</sup> for LCO, NCM and LFMCP, respectively). **(c, d)** Galvanostatic cycling tests in lithium half-cell at a C/2 rate for LCO and NCM and at a C/5 rate for LFMCP in terms of **(c)** voltage profiles at the 12<sup>th</sup> cycle and **(d)** cycling trend (specific capacity and Coulombic efficiency on the left and right y-axes, respectively).

Three full-cells combining the MWCNT<sup>+</sup> anode with the LCO, NCM and LFMCP materials, respectively, have been assembled. The cells had an excess of anode capacity in order to balance the first-cycle irreversible capacity of the cathodes and avoid possible lithium plating

at the negative electrode (see the Experimental section for further details).<sup>1</sup> Moreover, the negative electrodes were pre-cycled and partially lithiated, as described in the Experimental section. Such an approach allowed the formation of the SEI over the anode surface without any loss of lithium at the cathode side.<sup>54</sup>

Fig. 5 compares the galvanostatic cycling responses of the full-cells in terms of voltage profiles (panel a) and cycling behavior (panel b). The lower working voltage and the additional slope observed of the full-cells (Fig. 5a) with respect to LCO, NCM and LFMCP in the corresponding half-cells (compare Fig. 4c and Fig. 5a) reflect the combination of the electrochemical processes at the negative and positive sides. The MWCNT'/LCO cell delivers a reversible capacity with respect to the cathode mass of  $103 \text{ mAh g}^{-1}$  at the first cycle though a voltage plateau at 3.8 V (Fig. 5a) and a capacity fading of 22% at the 40<sup>th</sup> cycle (Fig. 5b). Instead, the MWCNT'/NCM cell ensures very stable cycling trend with voltage profiles centered at 3.8 V and reversible capacity with respect to the cathode mass approaching  $150 \text{ mAh g}^{-1}$ . The high working voltage of the  $\text{Co}^{3+}/\text{Co}^{2+}$  couple (4.74 V vs  $\text{Li}^+/\text{Li}$  upon oxidation) leads to some electrolyte decomposition upon charge of both the half and full-cells using LFMCP.<sup>36,55</sup> Accordingly, the full-cell employing LFMCP exhibits lower Coulombic efficiency than those using LCO and NCM. The former cell reveals an initial reversible capacity with respect to the cathode mass of about  $110 \text{ mAh g}^{-1}$  which decreases to about  $64 \text{ mAh g}^{-1}$  at the 40<sup>th</sup> cycle, that is, the 58% of the initial capacity. This trend suggests the use of a more appropriate electrolyte for allowing efficient operation of the promising MWCNT'/LFMCP cell.

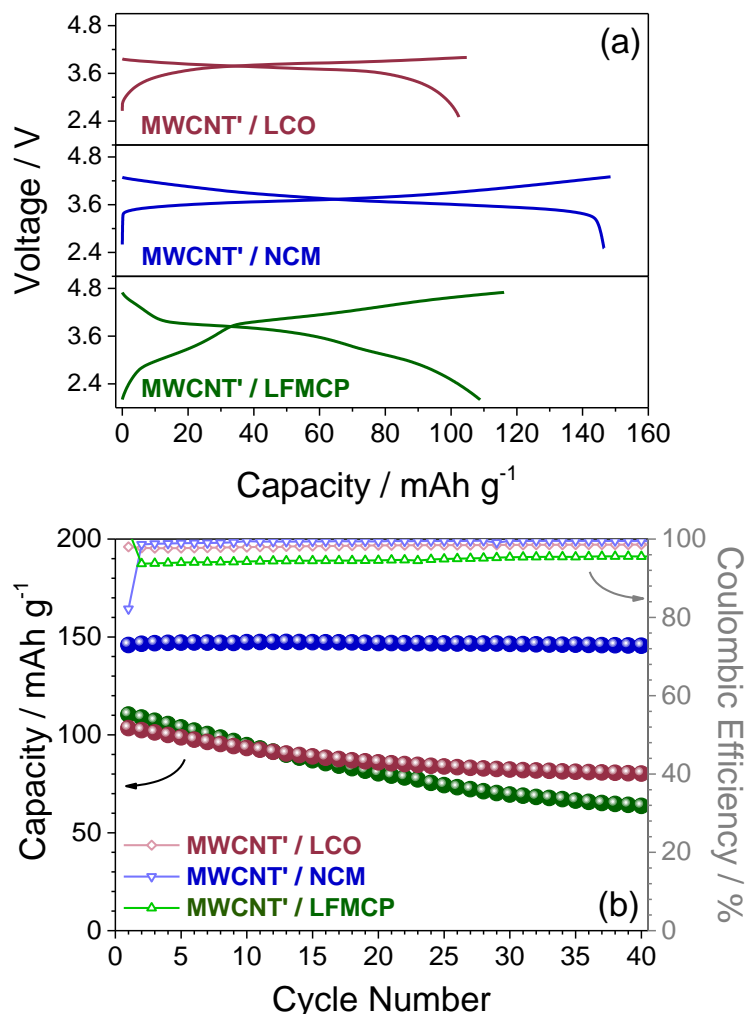


**Figure 5.** Galvanostatic cycling tests of full-cells using MWCNT' anode and LCO, NCM and LFMCP cathodes, respectively, in terms of (a) voltage profiles at the 2<sup>nd</sup> cycle and (b) cycling trend (specific capacity and Coulombic efficiency on the left and right y-axes, respectively). The specific capacity is referred to the cathode mass. MWCNT'/LCO cell: cycling within the 2.5 – 4 V range at a C/2 rate (137 mA g<sup>-1</sup> with respect to the cathode); MWCNT'/NCM cell: cycling within the 2.5 – 4.3 V range at a C/2 rate (140 mA g<sup>-1</sup> with respect to the cathode); MWCNT'/LFMCP cell: cycling within the 2 – 4.7 V range at a C/2 rate (85 mA g<sup>-1</sup>).

In summary, the MWCNT'/NCM full-cell has the most stable cycling trend. On the other hand, the full-cells using LCO and LFMCP exhibit a more pronounced capacity fading upon 40

cycles, which is likely related to the relatively low Coulombic efficiency. Indeed, the full-cells show average Coulombic efficiency values after the 5<sup>th</sup> cycle of 98.3% (LCO), 99.4% (NCM) and 94.9% (LFMCP; see Fig. 5b). It is noteworthy that the corresponding lithium half-cells employing LCO, NCM and LFMCP show comparable cycling stability despite the different Coulombic efficiency values, which are about 99% for LCO and NCM and 95% for LFMCP (see Fig. 4d), since the cells have an excess of lithium-metal anode. Accordingly, the observed capacity fading of lithium-ion cells may be reasonably attributed to loss of the cell balance upon cycling in view of electrolyte decomposition which is strongly related with the adopted cathode material.<sup>1</sup>

## Conclusion

Multiwalled carbon nanotubes electrode was fully characterized and used as the anode in combination with three cathodes, namely LCO, NCM and LFMCP. The carbon material had a partially graphitic structure, revealed by XRD and TEM-SADP, and was homogeneously formed by micrometric tubes with nanometric diameter (100 – 200 nm), as revealed by SEM and TEM. Such structural and morphological features ensured a stable capacity in lithium half-cell approaching 380 mAh g<sup>-1</sup> at 124 mA g<sup>-1</sup>, mostly delivered through electrochemical reactions below 0.5 V vs Li<sup>+</sup>/Li, as demonstrated by galvanostatic cycling and cyclic voltammetry. The electrode showed small voltage hysteresis and Coulombic efficiency of about 99.6%, *i.e.*, suitable features for full-cell application. The cathodes had different structural, morphological and electrochemical characteristics, herein investigated by XRD, SEM, SEM-EDS, cyclic voltammetry and galvanostatic cycling, which allowed full-cell study of the MWCNT' material in different electrochemical conditions. The layered LCO electrode reversibly (de)intercalated lithium at about 4 V vs Li<sup>+</sup>/Li within the hexagonal Li<sub>1-x</sub>CoO<sub>2</sub> phase, exhibiting the known

structural degradation due to phase transition above 4.1 V vs Li<sup>+</sup>/Li ( $x > 0.5$ ). Accordingly, the MWCNT'/LCO cell had a working voltage of 3.8 V, which is close to the charge cutoff (4 V), and delivered a reversible capacity of 103 mAh g<sub>cathode</sub><sup>-1</sup>. However, a low Coulombic efficiency value (lower than 99%) led to capacity fading of 22% after 40 cycles. Instead, the wide working voltage of NCM allowed for the MWCNT'/NCM cell high reversible capacity, *i.e.*, of about 150 mAh g<sub>cathode</sub><sup>-1</sup>, relevant Coulombic efficiency (above 99%), and very stable cycling. As for LFMCP, the high working voltage of the Co<sup>3+</sup>/Co<sup>2+</sup> couple (4.74 V vs Li<sup>+</sup>/Li upon charge), lowered the Coulombic efficiency to about 95%, and affected the electrode balance upon cycling in full-cell. Indeed, the MWCNT'/LFMCP battery delivered an initial capacity of 110 mAh g<sub>cathode</sub><sup>-1</sup> within the wide voltage range between 2 and 4.7 V, which dropped to 64 mAh g<sup>-1</sup> by 40 cycles. A more appropriate electrolyte was suggested as possible solution to this issue. Therefore, our results reveal the crucial role of the cathode in terms of working voltage for ensuring reversible full-cell operation whenever an anode with wider electrochemical potential window than graphite is used. Beside the small number of literature reports demonstrating the use of CNT anodes in lithium-ion full-cells,<sup>25,28</sup> Li-ion cells using MWCNTs anode and the various cathodes are herein shown for the first time. Hence, our study provides further insight into the application of CNT-based anodes in lithium-ion battery.

## Acknowledgements

This work was performed within the collaboration project “Accordo di Collaborazione Quadro 2015” between the University of Ferrara (Department of Chemical and Pharmaceutical Sciences) and the Sapienza University of Rome (Department of Chemistry), and partially founded by the grant “Fondo di Ateneo per la Ricerca Locale (FAR) 2017”. The authors thank Dr. Daniela Palmeri of the Electron Microscopy Centre, Department of Chemical and Pharmaceutical

Sciences, University of Ferrara, for recording SEM and TEM images, and Dr. Lorenza Marvelli for the FI-IR spectra.

### Supporting Information

Fig. S1 Schematic diagram of the T-type cell. Fig. S2 FT-IR spectra of pristine MWCNT and annealed MWCNT'. Fig. S3 Voltage profiles related to the rate capability test of MWCNT' in lithium half-cell. Fig. S4 Half-cell performances of pristine MWCNT and MWCNT'. Fig. S5 Voltage profiles related to the rate capability tests of LCO, NCM and LFMCP in lithium half-cell. This material is available free of charge via the Internet at <http://pubs.acs.org>.

### References

- (1) Di Lecce, D.; Verrelli, R.; Hassoun, J. Lithium-ion batteries for sustainable energy storage: recent advances towards new cell configurations. *Green Chem.* **2017**, *19* (15), 3442–3467. DOI: 10.1039/C7GC01328K.
- (2) Jun, D.-W.; Yoon, C. S.; Kim, U.-H.; Sun, Y.-K. High-Energy Density Core–Shell Structured Li[Ni<sub>0.95</sub>Co<sub>0.025</sub>Mn<sub>0.025</sub>]O<sub>2</sub> Cathode for Lithium-Ion Batteries. *Chem. Mater.* **2017**, *29* (12), 5048–5052. DOI: 10.1021/acs.chemmater.7b01425.
- (3) Verrelli, R.; Scrosati, B.; Sun, Y.; Hassoun, J. Stable, High Voltage Li<sub>0.85</sub>Ni<sub>0.46</sub>Cu<sub>0.1</sub>Mn<sub>1.49</sub>O<sub>4</sub> Spinel Cathode in a Lithium-Ion Battery Using a Conversion-Type CuO Anode. *ACS Appl. Mater. Interfaces* **2014**, *6* (7), 5206–5211. DOI: 10.1021/am500499a.
- (4) Sun, Y.-K.; Chen, Z.; Noh, H.-J.; Lee, D.-J.; Jung, H.-G.; Ren, Y.; Wang, S.; Yoon, C. S.; Myung, S.-T.; Amine, K. Nanostructured high-energy cathode materials for advanced lithium batteries. *Nat. Mater.* **2012**, *11* (11), 942–947. DOI: 10.1038/nmat3435.
- (5) Di Lecce, D.; Manzi, J.; Vitucci, F. M.; De Bonis, A.; Panero, S.; Brutti, S. Effect of the

- iron doping in LiCoPO<sub>4</sub> cathode materials for lithium cells. *Electrochim. Acta* **2015**, *185*, 17–27. DOI: 10.1016/j.electacta.2015.10.107.
- (6) Oh, S.-M.; Myung, S.-T.; Sun, Y.-K. Olivine LiCoPO<sub>4</sub>–carbon composite showing high rechargeable capacity. *J. Mater. Chem.* **2012**, *22* (30), 14932–14937. DOI: 10.1039/C2JM31933K.
- (7) Oh, S.-M.; Myung, S.-T.; Park, J. B.; Scrosati, B.; Amine, K.; Sun, Y.-K. Double-structured LiMn<sub>(0.85)</sub>Fe<sub>(0.15)</sub>PO<sub>4</sub> coordinated with LiFePO<sub>4</sub> for rechargeable lithium batteries. *Angew. Chemie Int. Ed.* **2012**, *51* (8), 1853–1856. DOI: 10.1002/anie.201107394.
- (8) Aravindan, V.; Lee, Y.-S.; Madhavi, S. Research Progress on Negative Electrodes for Practical Li-Ion Batteries: Beyond Carbonaceous Anodes. *Adv. Energy Mater.* **2015**, *5* (13), 1402225. DOI: 10.1002/aenm.201402225.
- (9) Hasa, I.; Hassoun, J.; Passerini, S. Nanostructured Na-ion and Li-ion anodes for battery application: A comparative overview. *Nano Res.* **2017**, *10* (12), 3942–3969. DOI: 10.1007/s12274-017-1513-7.
- (10) Hassoun, J.; Derrien, G.; Panero, S.; Scrosati, B. A Nanostructured Sn-C Composite Lithium Battery Electrode with Unique Stability and High Electrochemical Performance. *Adv. Mater.* **2008**, *20* (16), 3169–3175. DOI: 10.1002/adma.200702928.
- (11) Kim, C.; Ko, M.; Yoo, S.; Chae, S.; Choi, S.; Lee, E.-H.; Ko, S.; Lee, S.-Y.; Cho, J.; Park, S. Novel design of ultra-fast Si anodes for Li-ion batteries: crystalline Si@amorphous Si encapsulating hard carbon. *Nanoscale* **2014**, *6* (18), 10604–10610. DOI: 10.1039/C4NR02394C.
- (12) Elia, G. A.; Hassoun, J. A SiO<sub>x</sub>-Based Anode in a High-Voltage Lithium-Ion Battery.

- ChemElectroChem* **2017**, 4 (9), 2164–2168. DOI: 10.1002/celec.201700316.
- (13) Ngo, D. T.; Le, H. T. T.; Kim, C.; Lee, J.-Y.; Fisher, J. G.; Kim, I.-D.; Park, C.-J. Mass-scalable Synthesis of 3D Porous Germanium-Carbon Composite Particles as an Ultra-high Rate Anode for Lithium Ion Batteries. *Energy Environ. Sci.* **2015**, 8, 3577–3588. DOI: 10.1039/C5EE02183A.
- (14) Verrelli, R.; Hassoun, J.; Farkas, A.; Jacob, T.; Scrosati, B. A new, high performance CuO/LiNi<sub>0.5</sub>Mn<sub>1.5</sub>O<sub>4</sub> lithium-ion battery. *J. Mater. Chem. A* **2013**, 1 (48), 15329–15333. DOI: 10.1039/C3TA13960C.
- (15) Verrelli, R.; Hassoun, J. High-Capacity NiO-(Mesocarbon Microbeads) Conversion Anode for Lithium-Ion Battery. *ChemElectroChem* **2015**, 2 (7), 988–994. DOI: 10.1002/celec.201500069.
- (16) Zhuo, L.; Wu, Y.; Wang, L.; Ming, J.; Yu, Y.; Zhang, X.; Zhao, F. CO<sub>2</sub>-expanded ethanol chemical synthesis of a Fe<sub>3</sub>O<sub>4</sub>@graphene composite and its good electrochemical properties as anode material for Li-ion batteries. *J. Mater. Chem. A* **2013**, 1 (12), 3954–3960. DOI: 10.1039/C3TA01388J.
- (17) Aravindan, V.; Lee, Y.-S.; Madhavi, S. Best Practices for Mitigating Irreversible Capacity Loss of Negative Electrodes in Li-Ion Batteries. *Adv. Energy Mater.* **2017**, 7 (17), 1602607. DOI: 10.1002/aenm.201602607.
- (18) Gao, B.; Bower, C.; Lorentzen, J. D.; Fleming, L.; Kleinhammes, a.; Tang, X. P.; McNeil, L. E.; Wu, Y.; Zhou, O. Enhanced saturation lithium composition in ball-milled single-walled carbon nanotubes. *Chem. Phys. Lett.* **2000**, 327 (1–2), 69–75. DOI: 10.1016/S0009-2614(00)00851-4.
- (19) Mi, C. H.; Cao, G. S.; Zhao, X. B. A non-GIC mechanism of lithium storage in chemical

- etched MWNTs. *J. Electroanal. Chem.* **2004**, 562 (2), 217–221. DOI: 10.1016/j.jelechem.2003.09.004.
- (20) Eom, J. Y.; Kwon, H. S.; Liu, J.; Zhou, O. Lithium insertion into purified and etched multi-walled carbon nanotubes synthesized on supported catalysts by thermal CVD. *Carbon N. Y.* **2004**, 42 (12–13), 2589–2596. DOI: 10.1016/j.carbon.2004.05.039.
- (21) Wang, X. X.; Wang, J. N.; Chang, H.; Zhang, Y. F. Preparation of short carbon nanotubes and application as an electrode material in Li-ion batteries. *Adv. Funct. Mater.* **2007**, 17 (17), 3613–3618. DOI: 10.1002/adfm.200700319.
- (22) Zhou, J.; Song, H.; Fu, B.; Wu, B.; Chen, X. Synthesis and high-rate capability of quadrangular carbon nanotubes with one open end as anode materials for lithium-ion batteries. *J. Mater. Chem.* **2010**, 20 (14), 2794–2800. DOI: 10.1039/B926576G.
- (23) Chew, S. Y.; Ng, S. H.; Wang, J.; Novák, P.; Krumeich, F.; Chou, S. L.; Chen, J.; Liu, H. K. Flexible free-standing carbon nanotube films for model lithium-ion batteries. *Carbon N. Y.* **2009**, 47 (13), 2976–2983. DOI: 10.1016/j.carbon.2009.06.045.
- (24) Iijima, S. Helical microtubules of graphitic carbon. *Nature* **1991**, 354 (6348), 56–58. DOI: 10.1038/354056a0.
- (25) Landi, B. J.; Ganter, M. J.; Cress, C. D.; DiLeo, R. A.; Raffaele, R. P. Carbon nanotubes for lithium ion batteries. *Energy Environ. Sci.* **2009**, 2 (6), 638–654. DOI: 10.1039/B904116H.
- (26) De Las Casas, C.; Li, W. A review of application of carbon nanotubes for lithium ion battery anode material. *J. Power Sources* **2012**, 208, 74–85. DOI: 10.1016/j.jpowsour.2012.02.013.
- (27) Eom, J.; Kim, D.; Kwon, H. Effects of ball-milling on lithium insertion into multi-walled

- carbon nanotubes synthesized by thermal chemical vapour deposition. *J. Power Sources* **2006**, *157* (1), 507–514. DOI: 10.1016/j.jpowsour.2005.08.024.
- (28) Sehrawat, P.; Julien, C.; Islam, S. S. Carbon nanotubes in Li-ion batteries: A review. *Mater. Sci. Eng. B Solid-State Mater. Adv. Technol.* **2016**, *213*, 12–40. DOI: 10.1016/j.mseb.2016.06.013.
- (29) DiLeo, R. A.; Castiglia, A.; Ganter, M. J.; Rogers, R. E.; Cress, C. D.; Raffaele, R. P.; Landi, B. J. Enhanced Capacity and Rate Capability of Carbon Nanotube Based Anodes with Titanium Contacts for Lithium Ion Batteries. *ACS Nano* **2010**, *4* (10), 6121–6131. DOI: 10.1021/nn1018494.
- (30) Lahiri, I.; Oh, S.-W.; Hwang, J. Y.; Cho, S.; Sun, Y.-K.; Banerjee, R.; Choi, W. High Capacity and Excellent Stability of Lithium Ion Battery Anode Using Interface-Controlled Binder-Free Multiwall Carbon Nanotubes Grown on Copper. *ACS Nano* **2010**, *4* (6), 3440–3446. DOI: 10.1021/nn100400r.
- (31) Oktaviano, H. S.; Yamada, K.; Waki, K. Nano-drilled multiwalled carbon nanotubes: characterizations and application for LIB anode materials. *J. Mater. Chem.* **2012**, 25167–25173. DOI: 10.1039/C2JM34684B.
- (32) Chen, Y.; Li, X.; Park, K.; Song, J.; Hong, J.; Zhou, L.; Mai, Y. W.; Huang, H.; Goodenough, J. B. Hollow carbon-nanotube/carbon-nanofiber hybrid anodes for Li-ion batteries. *J. Am. Chem. Soc.* **2013**, *135* (44), 16280–16283. DOI: 10.1021/ja408421n.
- (33) Landi, B. J.; Ganter, M. J.; Schauerman, C. M.; DiLeo, R. A.; Cress, C. D.; Raffaele, R. P. Single Wall Carbon Nanotube – LiCoO<sub>2</sub> Lithium Ion Batteries. *MRS Proc.* **2008**, *1127* (figure 1), 1127-T03-6. DOI: 10.1557/PROC-1127-T03-06.
- (34) Ohzuku, T.; Ueda, A. Solid-State Redox Reactions of LiCoO<sub>2</sub> (R3m) for 4 Volt

- Secondary Lithium Cells. *J. Electrochem. Soc.* **1994**, *141* (11), 2972–2977. DOI: 10.1149/1.2059267.
- (35) Lee, M.-H.; Kang, Y.-J.; Myung, S.-T.; Sun, Y.-K. Synthetic optimization of Li[Ni<sub>1/3</sub>Co<sub>1/3</sub>Mn<sub>1/3</sub>]O<sub>2</sub> via co-precipitation. *Electrochim. Acta* **2004**, *50* (4), 939–948. DOI: 10.1016/j.electacta.2004.07.038.
- (36) Di Lecce, D.; Brescia, R.; Scarpellini, A.; Prato, M.; Hassoun, J. A High Voltage Olivine Cathode for Application in Lithium-Ion Batteries. *ChemSusChem* **2016**, *9* (2), 223–230. DOI: 10.1002/cssc.201501330.
- (37) Di Lecce, D.; Carbone, L.; Gancitano, V.; Hassoun, J. Rechargeable lithium battery using non-flammable electrolyte based on tetraethylene glycol dimethyl ether and olivine cathodes. *J. Power Sources* **2016**, *334*, 146–153. DOI: 10.1016/j.jpowsour.2016.09.164.
- (38) Carbone, L.; Di Lecce, D.; Gobet, M.; Munoz, S.; Devany, M.; Greenbaum, S.; Hassoun, J. Relevant Features of a Triethylene Glycol Dimethyl Ether-Based Electrolyte for Application in Lithium Battery. *ACS Appl. Mater. Interfaces* **2017**, *9* (20), 17085–17095. DOI: 10.1021/acsami.7b03235.
- (39) Arrebola, J. C.; Caballero, A.; Hernán, L.; Morales, J. Graphitized Carbons of Variable Morphology and Crystallinity: A Comparative Study of Their Performance in Lithium Cells. *J. Electrochem. Soc.* **2009**, *156* (12), A986. DOI: 10.1149/1.3231489.
- (40) Tehrani, M. S.; Azar, P. A.; Namin, P. E.; Dehaghi, S. M. Removal of Lead Ions from Wastewater Using Functionalized Multiwalled Carbon Nanotubes with Tris(2-Aminoethyl)Amine. *J. Environ. Prot.* **2013**, *4* (6), 529–536. DOI: 10.4236/jep.2013.46062.
- (41) Al-Shuja'a, O.; Obeid, A.; El-Shekeil, Y.; Hashim, M.; Al-Washali, Z. New Strategy for

- Chemically Attachment of Imine Group on Multi-Walled Carbon Nanotubes Surfaces: Synthesis, Characterization and Study of DC Electrical Conductivity. *J. Mater. Sci. Chem. Eng.* **2017**, *5* (2), 11–21. DOI: 10.4236/msce.2017.52002.
- (42) Periyasamy, T.; Asrafali, S. P.; Kim, S.-C. Functionalized MWCNTs, an efficient reinforcement for the preparation of eugenol based high performance PBz/BMI/CNT nanocomposites exhibiting outstanding thermo-mechanical properties. *New J. Chem.* **2017**, *41* (14), 6607–6615. DOI: 10.1039/C7NJ00357A.
- (43) Verma, P.; Maire, P.; Novák, P. A review of the features and analyses of the solid electrolyte interphase in Li-ion batteries. *Electrochim. Acta* **2010**, *55* (22), 6332–6341. DOI: 10.1016/j.electacta.2010.05.072.
- (44) Gauthier, M.; Carney, T. J.; Grimaud, A.; Giordano, L.; Pour, N.; Chang, H.-H.; Fenning, D. P.; Lux, S. F.; Paschos, O.; Bauer, C.; et al. Electrode–Electrolyte Interface in Li-Ion Batteries: Current Understanding and New Insights. *J. Phys. Chem. Lett.* **2015**, *6* (22), 4653–4672. DOI: 10.1021/acs.jpcclett.5b01727.
- (45) Winter, M.; Besenhard, J. O.; Spahr, M. E.; Novák, P. Insertion Electrode Materials for Rechargeable Lithium Batteries. *Adv. Mater.* **1998**, *10* (10), 725–763. DOI: 10.1002/(SICI)1521-4095(199807)10:10<725::AID-ADMA725>3.0.CO;2-Z.
- (46) Di Lecce, D.; Hassoun, J. Lithium Transport Properties in  $\text{LiMn}_{1-\alpha}\text{Fe}_\alpha\text{PO}_4$  Olivine Cathodes. *J. Phys. Chem. C* **2015**, *119* (36), 20855–20863. DOI: 10.1021/acs.jpcc.5b06727.
- (47) Di Lecce, D.; Hu, T.; Hassoun, J. Electrochemical features of  $\text{LiMnPO}_4$  olivine prepared by sol-gel pathway. *J. Alloys Compd.* **2017**, *693*, 730–737. DOI: 10.1016/j.jallcom.2016.09.193.

- (48) Uchida, I. Preparation of Binder-Free, Thin Film LiCoO<sub>2</sub> and Its Electrochemical Responses in a Propylene Carbonate Solution. *J. Electrochem. Soc.* **1995**, *142* (9), L139–L141. DOI: 10.1149/1.2048725.
- (49) Cho, J.; Kim, Y. J.; Park, B. Novel LiCoO<sub>2</sub> cathode material with Al<sub>2</sub>O<sub>3</sub> coating for a Li ion cell. *Chem. Mater.* **2000**, *12* (12), 3788–3791. DOI: 10.1021/cm000511k.
- (50) Yang, X. .; Sun, X.; McBreen, J. New phases and phase transitions observed in Li<sub>1-x</sub>CoO<sub>2</sub> during charge: in situ synchrotron X-ray diffraction studies. *Electrochem. commun.* **2000**, *2* (2), 100–103. DOI: 10.1016/S1388-2481(99)00155-1.
- (51) Sun, Y.-K.; Yoon, C. S.; Myung, S.-T.; Belharouak, I.; Amine, K. Role of AlF<sub>3</sub> Coating on LiCoO<sub>2</sub> Particles during Cycling to Cutoff Voltage above 4.5 V. *J. Electrochem. Soc.* **2009**, *156* (12), A1005–A1010. DOI: 10.1149/1.3236501.
- (52) Yang, S.; Wang, X.; Yang, X.; Liu, L.; Liu, Z.; Bai, Y.; Wang, Y. Influence of Li source on tap density and high rate cycling performance of spherical Li[Ni<sub>1/3</sub>Co<sub>1/3</sub>Mn<sub>1/3</sub>]O<sub>2</sub> for advanced lithium-ion batteries. *J. Solid State Electrochem.* **2012**, *16* (3), 1229–1237. DOI: 10.1007/s10008-011-1513-6.
- (53) Di Lecce, D.; Brutti, S.; Panero, S.; Hassoun, J. A new Sn-C/LiFe<sub>0.1</sub>Co<sub>0.9</sub>PO<sub>4</sub> full lithium-ion cell with ionic liquid-based electrolyte. *Mater. Lett.* **2015**, *139*, 329–332. DOI: 10.1016/j.matlet.2014.10.089.
- (54) Di Lecce, D.; Verrelli, R.; Campanella, D.; Marangon, V.; Hassoun, J. A New CuO-Fe<sub>2</sub>O<sub>3</sub>-Mesocarbon Microbeads Conversion Anode in a High-Performance Lithium-Ion Battery with a Li<sub>1.35</sub>Ni<sub>0.48</sub>Fe<sub>0.1</sub>Mn<sub>1.72</sub>O<sub>4</sub> Spinel Cathode. *ChemSusChem* **2017**, *10* (7), 1607–1615. DOI: 10.1002/cssc.201601638.
- (55) Xu, K. Nonaqueous Liquid Electrolytes for Lithium-Based Rechargeable Batteries. *Chem.*

*Rev.* **2004**, *104* (10), 4303–4418. DOI: 10.1021/cr030203g.

## Table of content image

Lithium-ion batteries combining MWCNTs anode with  $\text{LiCoO}_2$ ,  $\text{Li}[\text{Ni}_{1/3}\text{Co}_{1/3}\text{Mn}_{1/3}]\text{O}_2$  and  $\text{LiFe}_{1/4}\text{Mn}_{1/2}\text{Co}_{1/4}\text{PO}_4$  cathodes are originally studied as sustainable energy storage systems.

